JOURNAL OF GEOPHYSICAL RESEARCH, VOL. 115, A04304, doi:10.1029/2009JA014830, 2010

Longitudinal development of low-latitude ionospheric irregularities during the geomagnetic storms of July 2004

Guozhu Li,[1] Baiqi Ning,[1] Lianhuan Hu,[1] Libo Liu,[1] Xinan Yue,[1,2] Weixing Wan,[1] Biqiang Zhao,[1] K. Igarashi,[3] Minoru Kubota,[3] Yuichi Otsuka,[4] J. S. Xu,[5] and J. Y. Liu[6]

Received 24 August 2009; revised 12 October 2009; accepted 10 November 2009; published 1 April 2010.

[1] During the period 22–28 July 2004, three geomagnetic storms occurred due to a sequence of coronal mass ejections. In this paper we present and discuss the ionospheric observations from a set of in situ satellites and ground-based GPS total electron content and scintillation receivers, a VHF radar, and two chains of ionosondes (~300°E and ~120°E, respectively) that provide the evolutionary characteristics of equatorial and low-latitude ionospheric irregularities versus longitude during these storm periods. It is found that the irregularities occurred over a wide longitudinal range, extending from around 300°E to 120°E on storm days 25 and 27 July 2004. On 25 July plasma bubbles (PBs) began premidnight in America and postmidnight in Southeast Asia. On 27 July the occurrence of irregularities followed the sunset terminator and was observed sequentially after sunset from American to Southeast Asian longitudes. Past studies have reported that storm-time low-latitude ionospheric irregularities are mostly confined to a narrower longitude range, <90°, after sunset hours and are associated with the prompt penetration of eastward electric fields (PPEFs) into low latitudes. In June solstice months the occurrence of range-type spread *F* or PBs is very low in Southeast Asian and South American sectors. In contrast, the present results indicate that geomagnetic storms triggered the wide longitudinal development of PBs. In the American sector this was probably due to the effects of PPEFs on both storm days. However, in the Southeast Asian sector the PBs on the 2 days probably arose from disturbance dynamo electric field (DDEF), PPEF, and gravity wave seeding effects. This study further shows that under complex storm conditions, besides the long duration or multiple penetrations, the combined effects of PPEFs and DDEFs could result in a wide longitude extent of ionospheric irregularities at times.

Citation: Li, G., et al. (2010), Longitudinal development of low-latitude ionospheric irregularities during the geomagnetic storms of July 2004, *J. Geophys. Res.*, *115*, A04304, doi:10.1029/2009JA014830.

1. Introduction

[2] In the past decade there has been growing interest in the investigation of plasma bubble (PB)-associated irregularities, which often profoundly impact satellite communication and navigation systems and produce ionospheric scintillations. The basic mechanism of generation and development of low-latitude spread *F* is the gravitational Rayleigh—Taylor (R-T) instability and the instability **E** × **B** [*Kelley*, 1989]. The growth rate of the R-T instability depends on external driving forces such as neutral wind and electric and magnetic fields, together with background ionospheric properties, for example, the flux tube integrated Pedersen conductivity and upward plasma density gradients [*Sultan*, 1996]. A comprehensive representation of the instability mechanisms leading to spread *F* irregularity generation is shown in Figure 1 of *Abdu* [2001]. Until now, many aspects of spread *F* and PBs, such as statistics on the longitudinal and seasonal distribution and the dependence on solar and magnetic activity, have been reasonably studied on the basis of ground and in situ satellite measurements [e.g., *Kil and Heelis.*, 1998a; *McClure et al.*, 1998; *Huang et al.*, 2001; *Burke et al.*, 2004; *Park et al.*, 2005; *Su et al.*, 2008]. However, its day-to-day variability remains unresolved even after several decades of research [e.g., *Martinis et al.*, 2005; *Abalde et al.*, 2009; *Abdu et al.*, 2009; *Basu et al.*, 2009]. It is still not clear why irregularities do not occur every day during seasons of high spread *F* occurrence at a given longitude. However, spread *F* can occasionally be observed in low-occurrence seasons. From the viewpoint of day-to-day

[1]Beijing National Observatory of Space Environment, Institute of Geology and Geophysics, Chinese Academy of Sciences, Beijing, China.
[2]Also at University Corporation for Atmospheric Research, Boulder, Colorado, USA.
[3]National Institute of Information and Communications Technology, Koganei, Japan.
[4]Solar-Terrestrial Environment Laboratory, Nagoya University, Nagoya, Japan.
[5]School of Electronic Information, Wuhan University, Wuhan, China.
[6]Institute of Space Science, National Central University, Chung-Li, Taiwan.

0148-0227/10/2009JA014830

variability, equatorial spread *F* (ESF) appears to be unrelated to the postsunset rise of the *F* layer [*Tsunoda*, 2006], although the events are well correlated climatologically [e.g., *Fejer et al.*, 1999; *Li et al.*, 2007]. To improve our understanding of this aspect, it may be helpful to investigate the storm-time generation and evolution of ESF and PBs, since potential source characteristics can be identified more reliably under dramatic storm-time disturbances.

[3] During geomagnetic storms, the development or inhibition of low-latitude spread *F* is mainly controlled by perturbations of the zonal electric field at the equator due to the variable nature of the couplings between high and low latitudes, and it depends on the variations of magnetospheric and ionospheric parameters that affect the strength of the growth rate of the disturbed time instability [*Martinis et al.*, 2005]. Both the prompt equatorward penetration of magnetospheric or high-latitude electric fields and the ionospheric disturbance dynamo significantly alter ionospheric electric fields in the equatorial and low-latitude regions [*Fejer and Scherliess*, 1997]. Moreover, the transportation of energy from high latitudes in the form of changes in global wind pattern and traveling atmospheric disturbances (TADs) owing to Joule heating can also cause ionospheric perturbations [e.g., *Lee et al.*, 2004; *Ding et al.*, 2008; *Lei et al.*, 2008]. Recently, by virtue of the combination of ground and in situ satellite observations and model analysis, the generation and evolution of storm-time spread *F* and PB-associated irregularities have been characterized. It has been found that PBs can bifurcate to small-scale structures, updraft at supersonic speeds, and extend in latitude and longitude as big bubbles [e.g., *Aggson et al.*, 1992; *Kil et al.*, 2006; *Ma and Maruyama*, 2006; *Huang et al.*, 2007; *Huba and Joyce*, 2007]. On the contrary, investigation of the local-time- or longitude-dependent response of storm-time irregularities often shows substantial differences in irregularity activity at nearby longitude regions [e.g., *Basu et al.*, 2001a; *Sahai et al.*, 2005; *Sreeja et al.*, 2009]. However, *Tulasi Ram et al.* [2008] found an interesting case where the total longitudinal width of PBs was as large as about 92° during storm periods on 15–16 May 2005, which they attributed to the effects of prompt penetration of electric fields (PPEFs). Under long-duration penetration or long-lasting multiple penetration of the interplanetary electric field to the low-latitude ionosphere [e.g., *Huang et al.*, 2005; *Huang*, 2008; *Wei et al.*, 2008], if the local dusk period coincides with the prompt-penetration phase, the low-latitude ionosphere over a wide longitudinal sector will be susceptible to the development of spread *F*. As a result, much wider longitudinal PB occurrence probably can be sequentially observed under some conditions.

[4] In July 2004 three geomagnetic storms occurred because of a sequence of coronal mass ejections [*Zhang et al.*, 2007; *Pedatella et al.*, 2008]. Figure 1 presents the temporal variations of the interplanetary magnetic field (IMF) *Bz*, *AE*, *Kp*, and *Dst* indexes, during the storm period 22–28 July 2004. This storm period is unusual because three intense storms occurred in succession. Figure 1 indicates that for the first storm, with a storm sudden commencement at 1036 UT and storm main-phase onset at 1900 UT on 22 July, *Dst* reached a minimum of −101 nT at 0030 UT on 23 July and *Kp* reached 7. While the first storm was recovering, the next coronal mass ejection intensified the storm again, with the second main-phase onset at 2130 UT on July 24; *Dst* reached −148 nT at 1200 UT on 25 July, and *Kp* reached 8. The third storm began at 2249 UT on 26 July, with main-phase onset at 0500 UT on 27 July. A minimum *Dst* of −197 nT was reached at 1400 UT on 27 July and *Kp* reached 9. For storm-time PB occurrence, most previous studies have concentrated on the effect of superstorms, and little work has been done on the longitudinal development of equatorial and low-latitude ionospheric irregularities, especially during multi-geomagnetic-storm periods. The objective of this study, however, is to investigate the longitudinal development of low-latitude PBs and ionospheric scintillations during the sequence of geomagnetic storms on 22–28 July 2004 using multi-instrument observations. We focus mainly on the Southeast Asian/Australian and South American longitude sectors. Under quiet conditions the June solstice is a low-occurrence season of range-type spread *F*, topside PBs, and GPS amplitude scintillations at the two selected longitudes [e.g., *Abdu et al.*, 1981; *Sahai et al.*, 2004]. In this study we report a much wider-longitude occurrence of PB-associated irregularities during the two consecutive geomagnetic storms of 25 and 27 July. This provides a chance to study which mechanism can trigger a large longitude extent of ionospheric irregularities in the low-occurrence season. In the following sections, first we give a brief description of the data sets used in the present paper. Then we present the general characteristics of the PB occurrence during the storm periods and discuss the possible mechanisms responsible for the development of irregularities. Finally, we give the conclusion.

2. Data Set Description

[5] Ground-based GPS total electron content (TEC) and in situ satellite density measurements have been extensively used to study the global climatology of PB occurrence rates [e.g., *Kil and Heelis*, 1998b; *Su et al.*, 2006; *Nishioka et al.*, 2008]. In this study we also mainly use these observations to get an overview of the longitudinal development of storm-time ionospheric irregularities. We use TEC data from the Crust Movement Observation Network of China (CMONOC) and International Global Navigation Satellite System Service (IGS) GPS receivers at low latitudes to measure the TEC index [*Pi et al.*, 1997] and obtain a PB occurrence rate map in a manner similar to that used by *Li et al.* [2009]. Briefly, within a quadrate grid of 5° in geographic longitude and 1° in latitude (locations of ionosphere penetration points), the number of samples with the rate of TEC change index (ROTI) at $\geq$0.075 TECU min^{-1} (1 TECU [total electron content unit] = 10^{16} el m^{-2}) [*Nishioka et al.*, 2008] is divided by the total number of ROTI samples to obtain the PB occurrence rate in that square area at nighttime and then obtain the grid map of PB occurrence rates. In Figure 2 the triangles in the bottom right map represent the location of selected GPS TEC receivers.

[6] Data from ionosonde, VHF radar, and GPS ionospheric scintillation measurements have been used to evaluate the storm-time development of PBs at American and Southeast Asian longitudes. Amplitude scintillation is monitored by computing the S_4 index, which is the standard deviation of the received power normalized by its mean

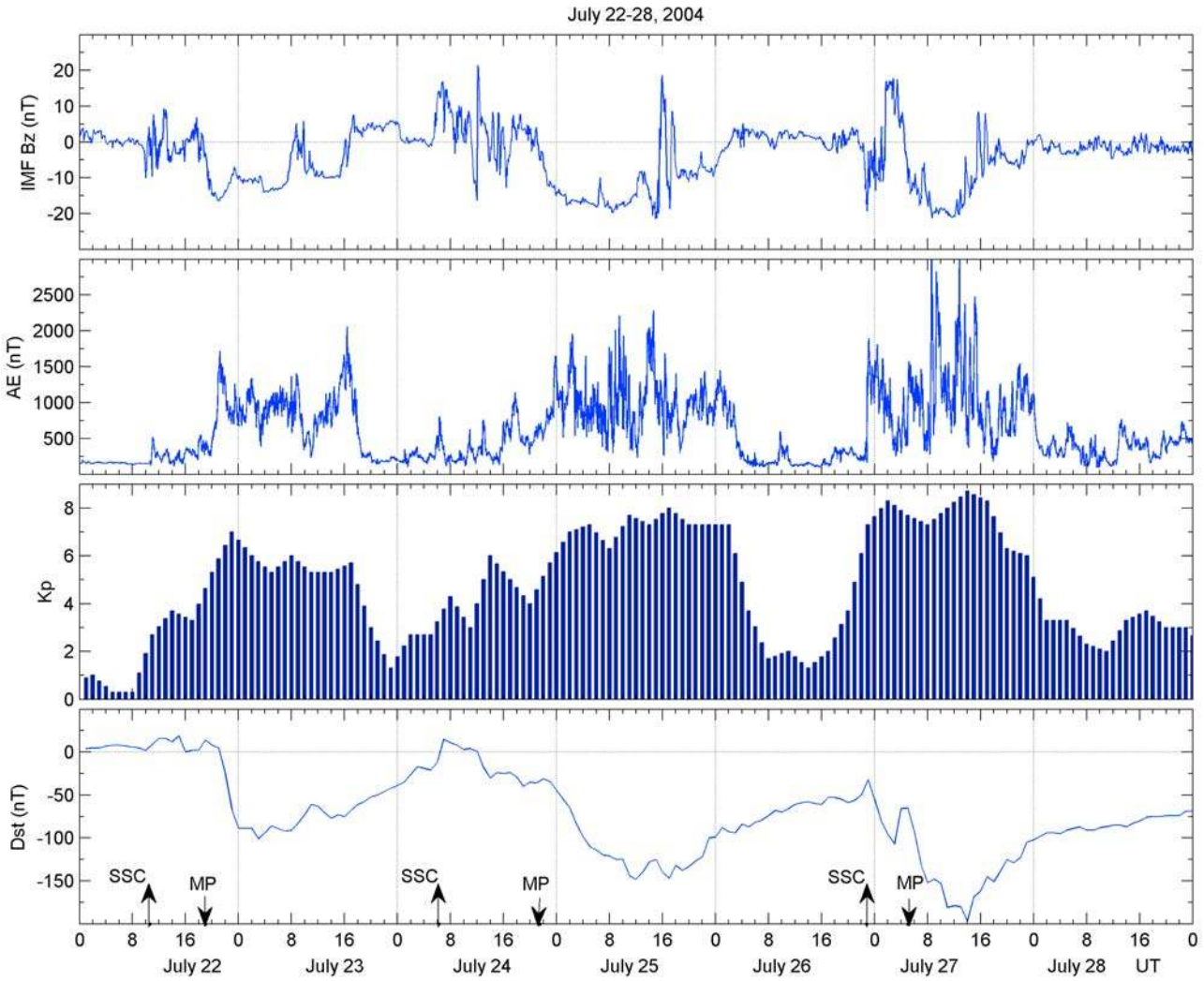

Figure 1. Interplanetary magnetic field (IMF) *Bz*, *AE*, *Kp*, and *Dst* indexes during the sequence of geomagnetic storms on 22–28 July 2004. Arrows in the bottom plot indicate the time of sudden storm commencement (SSC) and the main-phase (MP) onset time.

value, given by the equation $S_4^2 = (I^2 - I_{AV}^2)/(I_{AV}^2)$, where I is the instantaneous amplitude of the scintillation signal at each interval of the sampled time width, and I_{AV} is the averaged amplitude [*Briggs and Parkin*, 1963; *Dandekar and Groves*, 2004]. The scintillation receivers are set up in Wuhan and West Sumatra. To provide information on the generation and evolution of irregularities versus altitude in the South American longitude, we used the 50 MHz Jicamarca Unattended Long-Term Investigation (JULIA) radar to detect the plasma plume. The radar is operated at a peak power of 30 kW, and complete information is given by *Hysell and Burcham* [1998]. Furthermore, ionosonde data are obtained from two chains of ionosondes, consisting of Wuhan, Chungli, Learmonth, Darwin, and Cebu at the Southeast Asian/Australian longitude and Ascension Island, Fortaleza, and Jicamarca at the South American longitude. Details of observations made using these instruments are summarized in Table 1.

[7] On the contrary, we also use in situ plasma density measurements of the Defense Meteorological Satellite Program (DMSP) F15 and Challenging Minisatellite Payload (CHAMP) satellites, which orbit at about 800 and 380 km altitude, respectively, to support the PB observations identified by ground-based GPS TEC measurements, since the observed plasma density depletions from in situ satellites are the signatures of topside ionospheric irregularities. Detailed information about the satellites and the instruments onboard them are given in *Rich and Hairston* [1994] and *McNamara et al.* [2007].

3. Overview of the 22–28 July 2004 Plasma Bubble Events

[8] Many related references have pointed out that sharp TEC depletion can be ascribed to ionospheric PBs or plumes [e.g., *Kelley*, 1989; *Bhattacharyya et al.*, 2000] and to range-type spread F [*Lee et al.*, 2009]. A global representation of low-latitude nighttime PB occurrence rates using GPS TEC measurements during the storm period of 22–28 July 2004 is presented in Figure 2. The percentage occur-

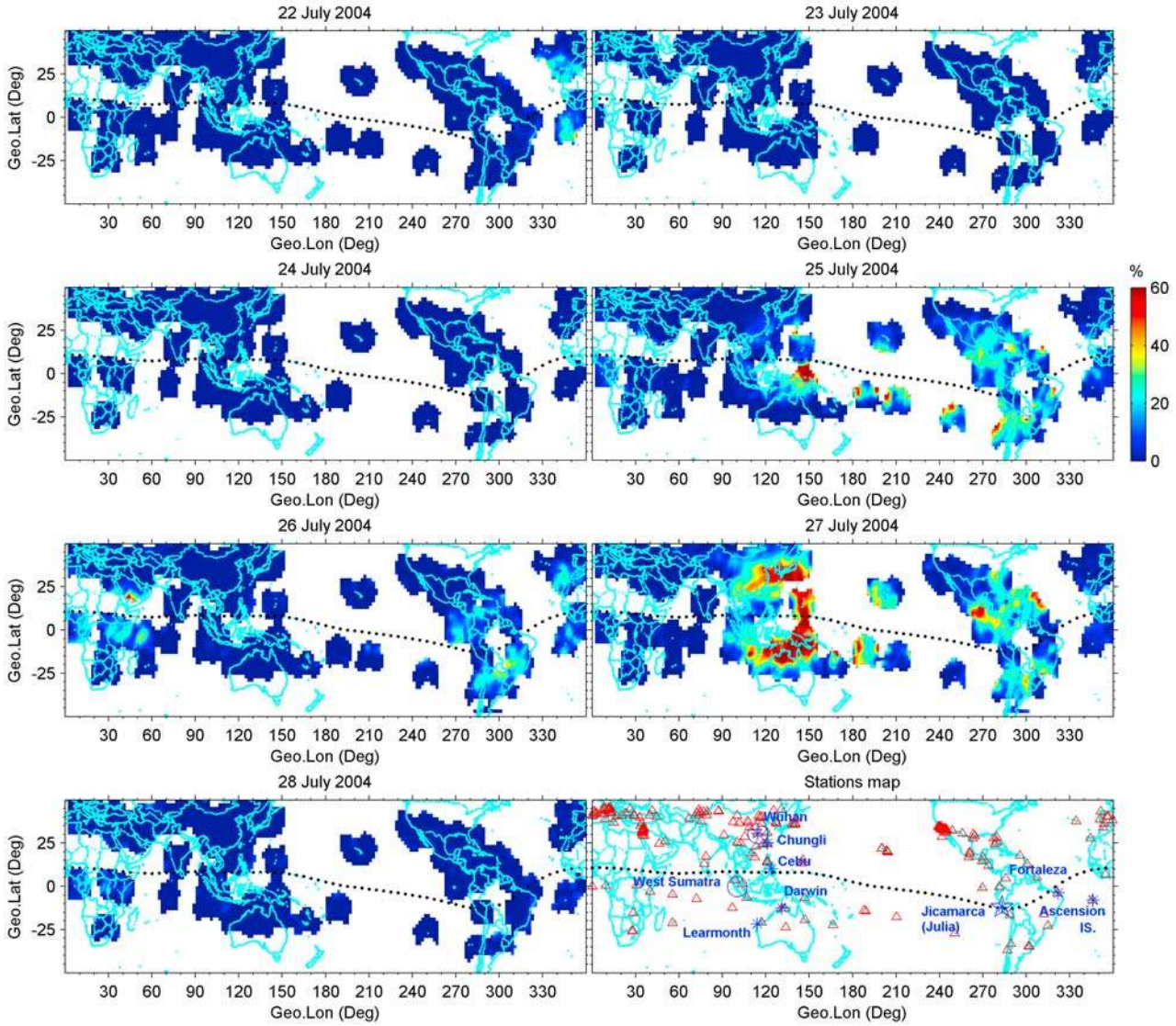

Figure 2. Maps of plasma bubble occurrence rates during the storm period 22–28 July 2004 obtained from ground-based GPS total electron content (TEC) receivers. The bottom right plot shows the geographical distribution of the GPS TEC (triangles) and scintillation receivers (open circles), ionosondes (asterisks), and VHF radar (star).

rence of irregularities at approximate locations is color-coded. The blank areas in the grid maps indicate that fewer than 30 ROTI samples for each grid are available in these regions. For the first storm day, 22 July, the top left map in Figure 2 shows that sharp TEC depletions occurred around 340°E, which could be associated with the prompt-penetration phase under the southward orientation of IMF *Bz*. A prominent feature observed in the TEC fluctuations can be clearly seen in the second and third maps on the right, which signify that PBs were observed on storm days 25 and 27 July 2004 over a wide longitude extent from east to west, around 300°E-120°E. As pointed out by *Basu et al.* [2005] and *Martinis et al.* [2005], the development or inhibition of ESF during geomagnetic storms is mainly controlled by perturbations of the zonal electric field. The local time dependence of the polarity and amplitude of electric per-

Table 1. Information on Stations Whose GPS Scintillation and Ionosonde Ionogram Data Were Used in This Study

Station	Geographic Latitude (deg)	Geographic Longitude (deg)	Magnetic Latitude (deg)	Resolution (min)
	Ionosonde Data			
Wuhan	30.5	114.4	20.3	15
Chungli	25.0	121.2	14.9	15
Learmonth	−21.8	114.1	−32.0	15
Darwin	−12.5	131.0	−22.4	5
Cebu	10.3	123.9	2.5	5
Jicamarca	−12.0	283.2	0.5	15
Fortaleza	−3.8	322.0	−5.1	10
Ascension Island	−8.0	346.0	−17.7	15
	Scintillation Data			
Wuhan	30.5	114.4	20.3	1
West Sumatra	−0.2	100.3	−9.3	1

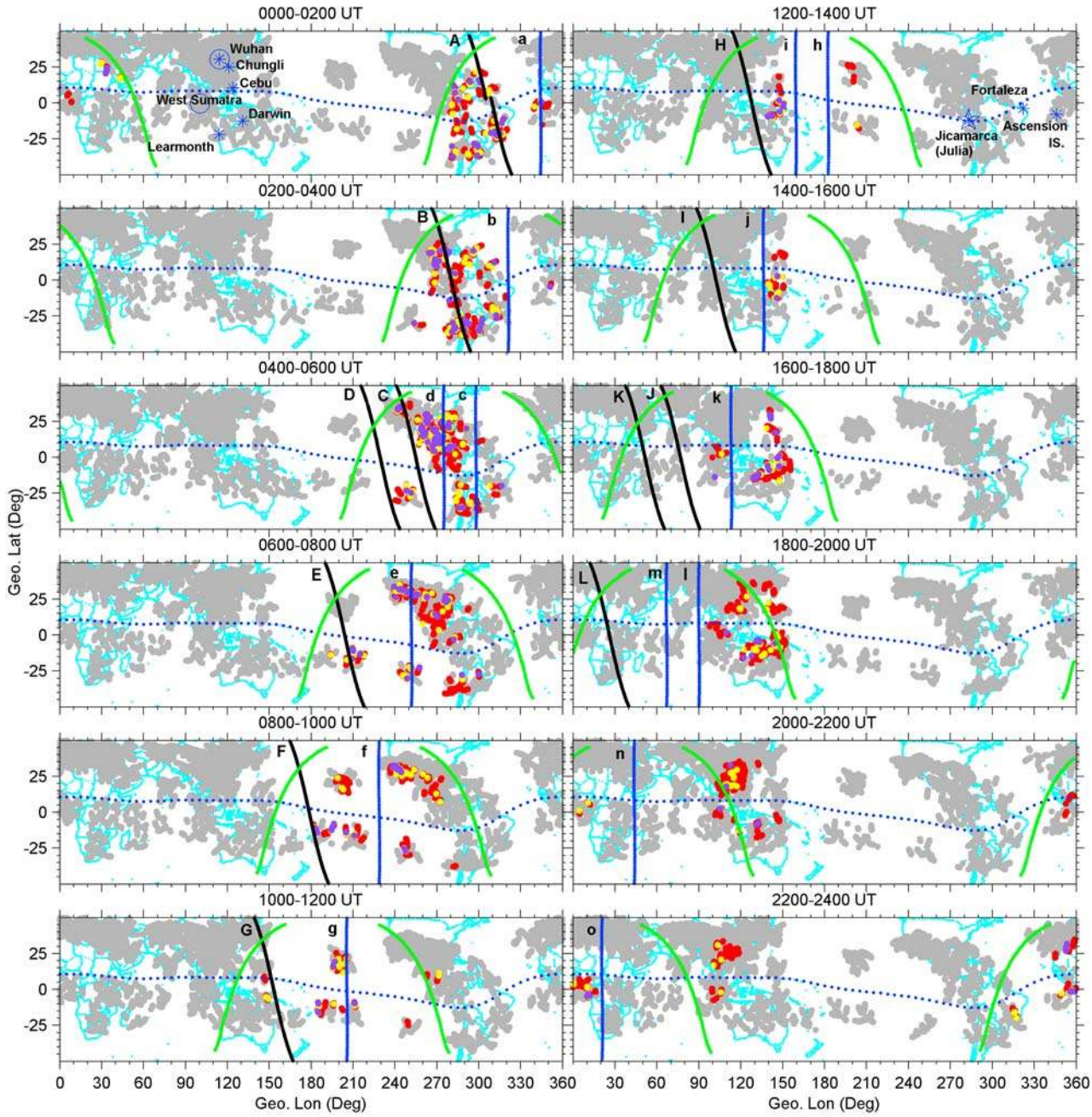

Figure 3. Sequence of rate of TEC change index (ROTI) maps on 25 July 25 2004. Red, yellow, and purple areas represent the ROTI above the threshold 0.075, 0.3, and 0.5 TECU min^{-1} (1 TECU (TEC unit) = 10^{16} el m^{-2}), respectively. Green lines in each plot show the sunset (SS) and sunrise (SR) terminator. Black and blue lines show the ground tracks of F15 and CHAMP orbits crossing the area, labeled A–L and a–o, respectively. Corresponding density measurements along the satellite tracks are shown in Figure 4. The thin dashed line represents the dip equator.

turbations determines the favorable or unfavorable conditions at any given location [*Tulasi Ram et al.*, 2008]. Many cases are similar to that of 22 July, in that the irregularities occur over a narrower longitude range and the local dusk period coincides with the prompt-penetration phases [e.g., *Basu et al.*, 2005; *Abdu et al.*, 2008]. An eastward PPEF present at dusk hours could lift the *F* layer to a high enough altitude and cause growth of instability by the R-T mechanism, leading to the development or intensification of spread *F*. However, when the sunset terminator crosses the adjacent longitude regions, the PPEF may be decayed or diminished and the eastward electric field may not be strong enough to elevate the *F* layer to a higher altitude and satisfy the conditions for generation of spread *F* or PBs. In the following we mainly focus our attention on investigating the development of irregularities on 25 and 27 July.

[9] We now consider the UT dependence of longitudinal development of PBs. Figures 3 and 5 give a sequence of

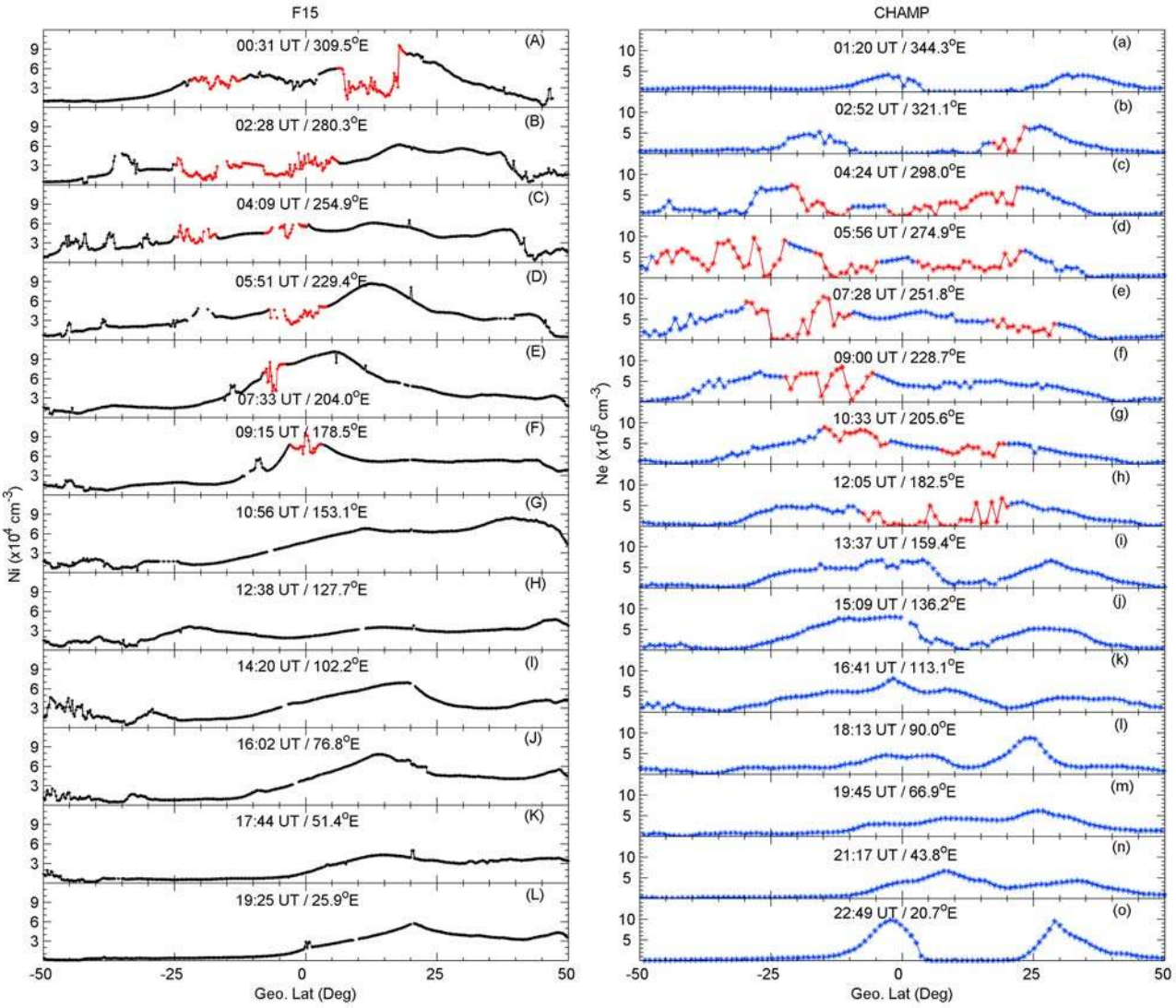

Figure 4. In situ plasma density measurements along the satellites (left) F15 and (right) CHAMP orbits. The equator-crossing longitude and time are also shown in each plot. Ground tracks of both satellites are shown in Figure 3.

ROTI maps at 2-h intervals on 25 and 27 July, respectively, plotted as a function of geographic longitude and latitude. The bold dots identified below in these plots represent the intersections of the raypaths from the GPS satellites to the ground stations with the *F* region at 400 km altitude. Some caution is required when studying the morphology, because a radio ray at lower elevation angles travels longer horizontal distances [*Pi et al.*, 1997]. In this study the elevation angle is confined to be greater than 15°, and the irregularity locations under such conditions give only a relative estimation. The red, yellow, and purple dots represent the ROTI above thresholds of 0.075, 0.3, and 0.5 TECU min^{-1}, respectively. The consecutive orbits of the DMSP F15 (labeled A–L) and CHAMP (labeled a–o) satellites are also shown superimposed on the maps. As shown in Figures 1 and 3, after the southward turning of the IMF *Bz* (~2200 UT on 24 July) and the abrupt increase in *AE* (~0000 UT on 25 July), irregularities can be seen at low latitudes in the American sector during 0000–0800 UT near postsunset. About 6 h later the magnetic storm went into a deep main phase and at 0600 UT *Dst* reached over ¯100 nT; development of ionospheric irregularities was recorded in the low-latitude Pacific regions premidnight (~0600–1200 UT) on 25 July. The IMF *Bz* turned northward at ~1550 UT on 25 July and remained there for 2 h. After that, PBs seemed to occur over the Southeast Asian/Australian sector postmidnight and persisted for several hours, until sunrise. Corresponding density data measured from the F15 and CHAMP satellites on the storm day are shown in Figure 4. They are used to verify PB development at the American and Pacific longitudes. Noticeably, as shown in the left plots in Figure 4, F15 detected multiple plasma density depletions within geographic latitude 25°S–25°N and longitude 300°–200°E, marked by the red lines in the density plots for orbits A–F around 0030–0900 UT. The CHAMP observations also show large density depletions in the consecutive passes (orbits b–h) from 0250 to 1200 UT. These density depletions were found to exist within the regions of

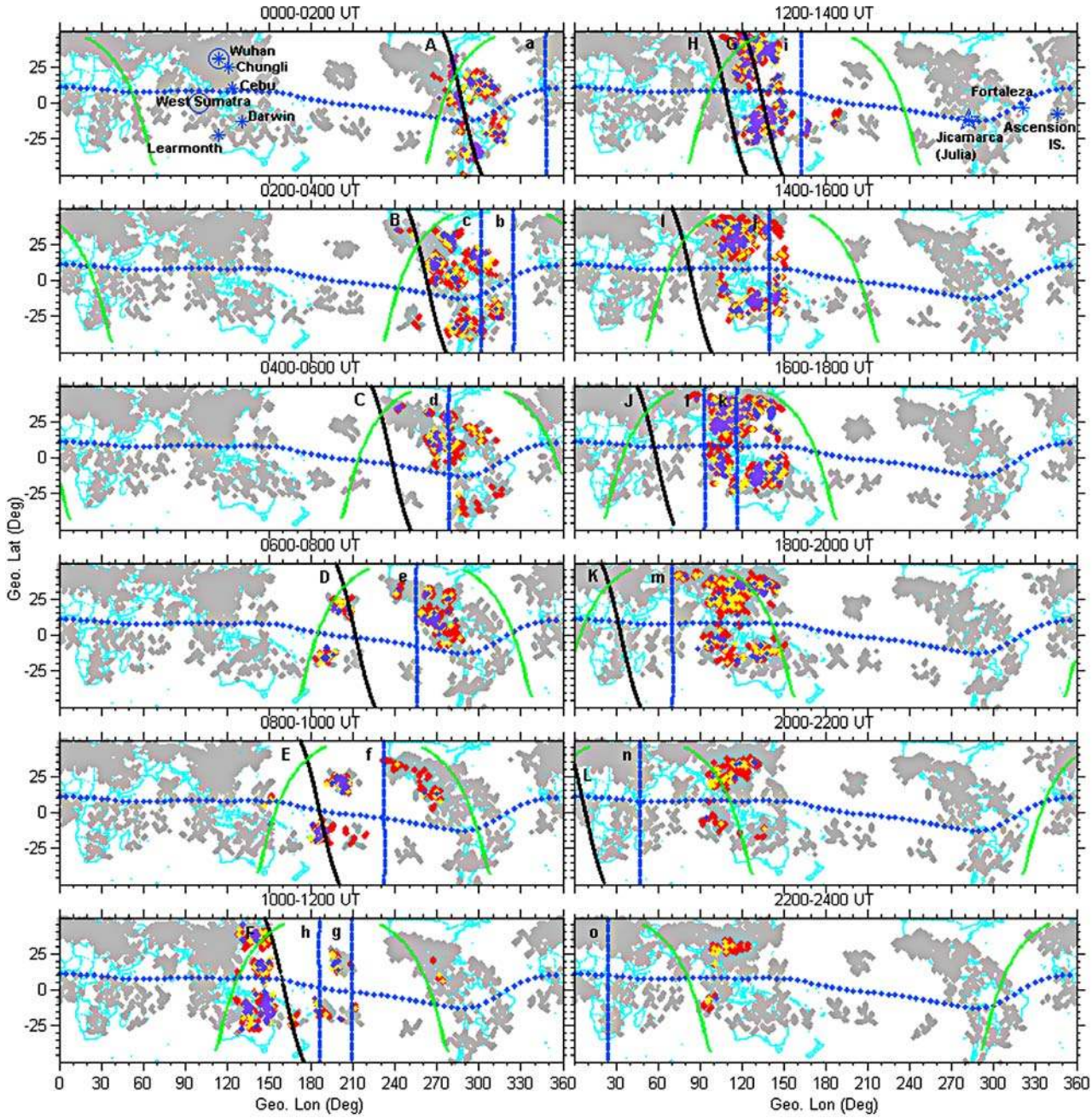

Figure 5. Same as Figure 3 but for July 27.

PB occurrence seen from the ROTI maps in Figure 3. Also, we note a disagreement: the absence versus presence of PBs from satellite density (orbits G–I for F15 and orbits k and l for CHAMP) versus GPS TEC measurements at Southeast Asian longitudes. This is because the PBs were initiated postmidnight, after the satellite passing time.

[10] Similarly, we now provide the longitudinal distribution of irregularities observed during 27 July. At American and Pacific longitudes, the characteristics of PB occurrence are similar to those on 25 July. As shown in Figures 5 and 6, irregularities were first seen at the American longitude at about 0000–0600 UT in the prompt-penetration phase of the storm. Local times at these longitudes were between 1900 and 0300 LT. From then on, bubble occurrence expanded westward and was observed at 0600–1200 UT in the Pacific regions. In the Southeast Asian/Australian sector, PBs were seen to initiate at 1000 UT, corresponding to 1900 LT (the irregularities seen before sunset during 0800–1200 UT are due to the 2-h UT window). The PB occurrence seen at this longitude is much wider than that on 25 July, extending from low to middle latitudes, and intense GPS amplitude scintillations were found (reported in section 4). The possible cause of this discrepancy is discussed in section 5. During the successive hours 1400 to 2400 UT, F15 orbits H–L and CHAMP orbits l–o crossed the western longitude of 90°E and showed an absence of density depletions. Taken

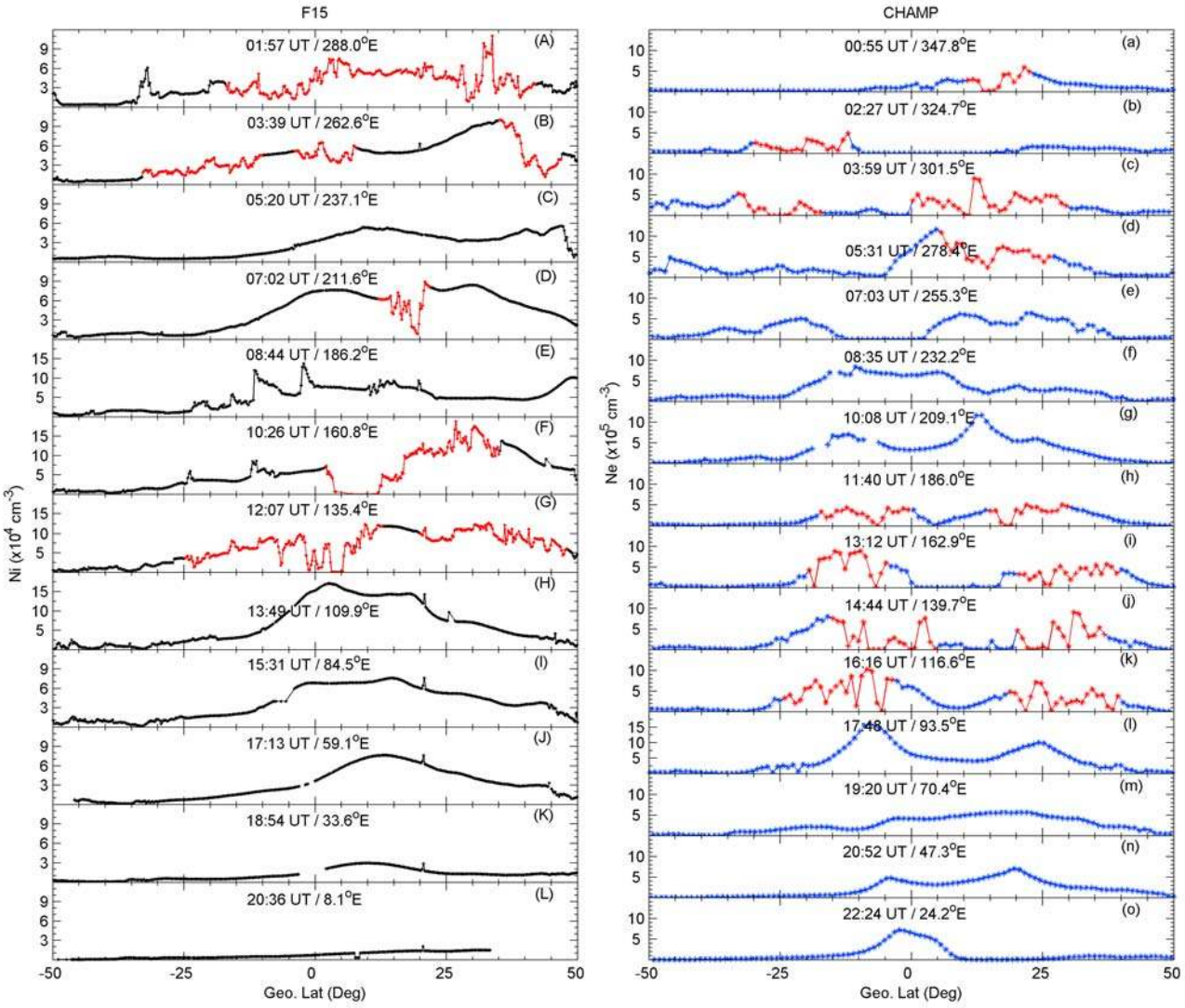

Figure 6. Same as Figure 4 but for July 27.

together, the ground-based GPS TEC and in situ density observations in Figures 3–6 offer convincing evidence that on storm days 25 and 27 July 2004, ionospheric irregularities occurred over a wider longitudinal extent. They started to develop at postsunset in the American and Pacific sectors, following a southward turning of the IMF *Bz* and intensification of *AE*. However, at Southeast Asian/Australian longitudes PBs started to develop postmidnight on 25 July (a northward turning of IMF *Bz*) and postsunset on 27 July (IMF remains southward), respectively, and both of them existed until sunrise. At local sunrise the development of a sunlit *E* layer would damp or prevent the development of ionospheric irregularities because of the much higher conductivity of the *E* layer [*Fukao et al.*, 2003], but at times it takes several hours for the bubbles to decay; thus, they occur even after sunrise or in the daytime. At western longitudes of 90°E, PBs were absent from both in situ and ground-based observations.

[11] For South American and Southeast Asian longitudes, the June solstice is the low-occurrence season of spread *F* [e.g., *Abdu et al.*, 1981; *Sahai et al.*, 2000] and plasma density depletion [e.g., *Park et al.*, 2005; *Su et al.*, 2006; *Li et al.*, 2007]. Using all-sky imaging measurements at 630 nm from year 1987 to year 2000 at Cachoeira Paulista (geographic longitude/latitude, 45.0°W/22.7°S; magnetic latitude, 16°S), *Sahai et al.* [2004] found only 12 nights with PBs present during the June solstice. Although the airglow observations were limited to clear nights (about 12 nights per month), the results are still amazing and indicate that June solstice is a season of low spread *F* occurrence. *Sastri et al.* [1997] statistically analyzed cases of such infrequent spread *F* occurrence and showed a high association with magnetically disturbed conditions. In section 4 we investigate the development of irregularities at the two longitudes in more detail and discuss possible mechanisms responsible for the occurrence of irregularities on storm days 25 and 27 July.

4. Evolution of Irregularities at South American Longitudes

[12] Investigating the variation of plasma drift will help to clarify the mechanisms that control the onset of spread *F*.

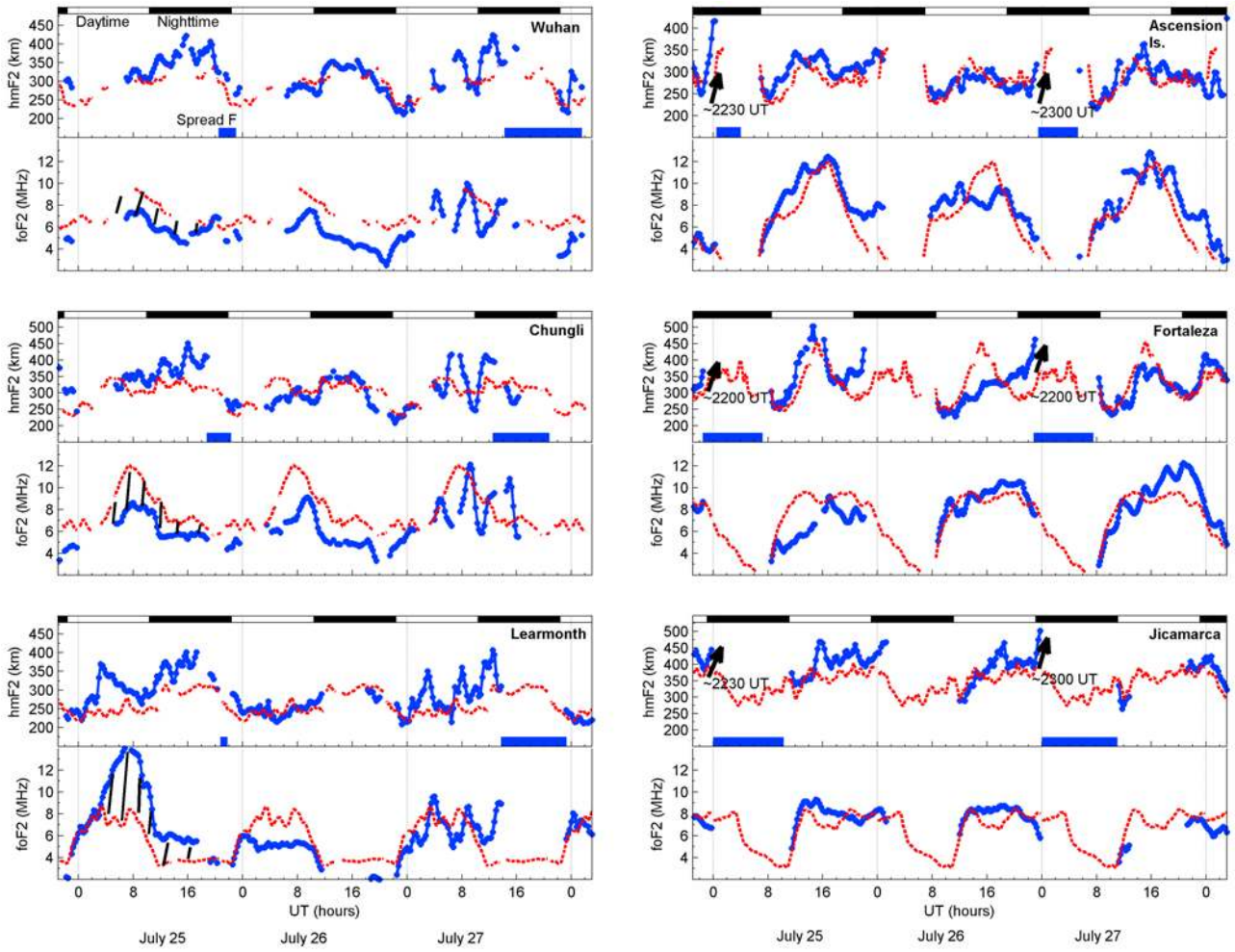

Figure 7. Variations of the ionospheric hmF2 and foF2 observed in the Southeast Asian/Australian (Wuhan, Chungli, and Learmonth) and South American (Ascension Island, Fortaleza, and Jicamarca) longitudinal sectors during 25–27 July 2004. Red lines are quiet-day (21 July 2004) values. Horizontal bars at the bottom of each plot indicate the duration of spread *F* (from ionograms) on 25 and 27 July. Top bars indicate daytime (white) and nighttime (black). Shaded areas in the left plots show negative/positive storms in the North/South Hemisphere, respectively. Arrows in right plots indicate prompt elevation of the *F* layer to a higher altitude at ~2230 UT on 24 July and 2300 UT on 26 July.

During storm periods, the most direct and easily observed effects of plasma drift are changes in the height of the *F* region [*Van Zandt et al.*, 1971; *Yue et al.*, 2008]. We analyzed ionosondes collecting ionograms at 15 min intervals at Ascension Island, Fortaleza, and Jicamarca and VHF coherent backscatter radar continuous observation by JULIA during the 2 storm days. Different types of range spread *F* (RSF) and frequency spread *F* on ionograms and radar plumelike signatures on range-time-intensity (RTI) maps of the VHF radar were observed. A description of spread *F* type and intensity is given by *Rodrigues et al.* [2004] and *Chen et al.* [2006].

[13] The right plots in Figure 7 show the hmF2 and foF2 variations at Ascension Island, Fortaleza, and Jicamarca. For comparison the diurnal variations on geomagnetic quiet day 21 July are denoted as thin dashed lines. The first, third, and fifth plots on the right show that on 24 July, hmF2 starts rising around 2200-2230 UT and goes up to ~420 km at Ascension Island, ~370 km at Fortaleza, and ~450 km at Jicamarca, respectively. Similar increases in the *F* layer are also seen on 26 July, at ~2300 UT. The near-simultaneous increases in the *F* layer on storm days indicate that an intensification in the eastward electric field occurred in the dusk sector, possibly due to the PPEF effect, which seems to follow a southward turning of the IMF *Bz* and a sudden increase in *AE* [*Kikuchi et al.*, 2000]. Indeed, *Pedatella et al.* [2008] recently used CHAMP observations to show a significantly enhanced electron density and expanse of EIA crests at ~0000 UT on 27 July. They speculated that the enhancement of EIAs may contribute to the eastward penetration electric field effects. Examination of the ionograms obtained at the three stations (not shown here) shows that the subsequent growth of range-type spread *F* is evident shortly after the time of an abrupt increase in *F* layer height, with a thickness of >300 km. For the first increase in *F* layer height on 24 July, the spread *F* observed at the three stations started at 0030 UT on 25 July, 2230 UT on 24 July, and 0000 UT on 25 July and lasted for about 4,

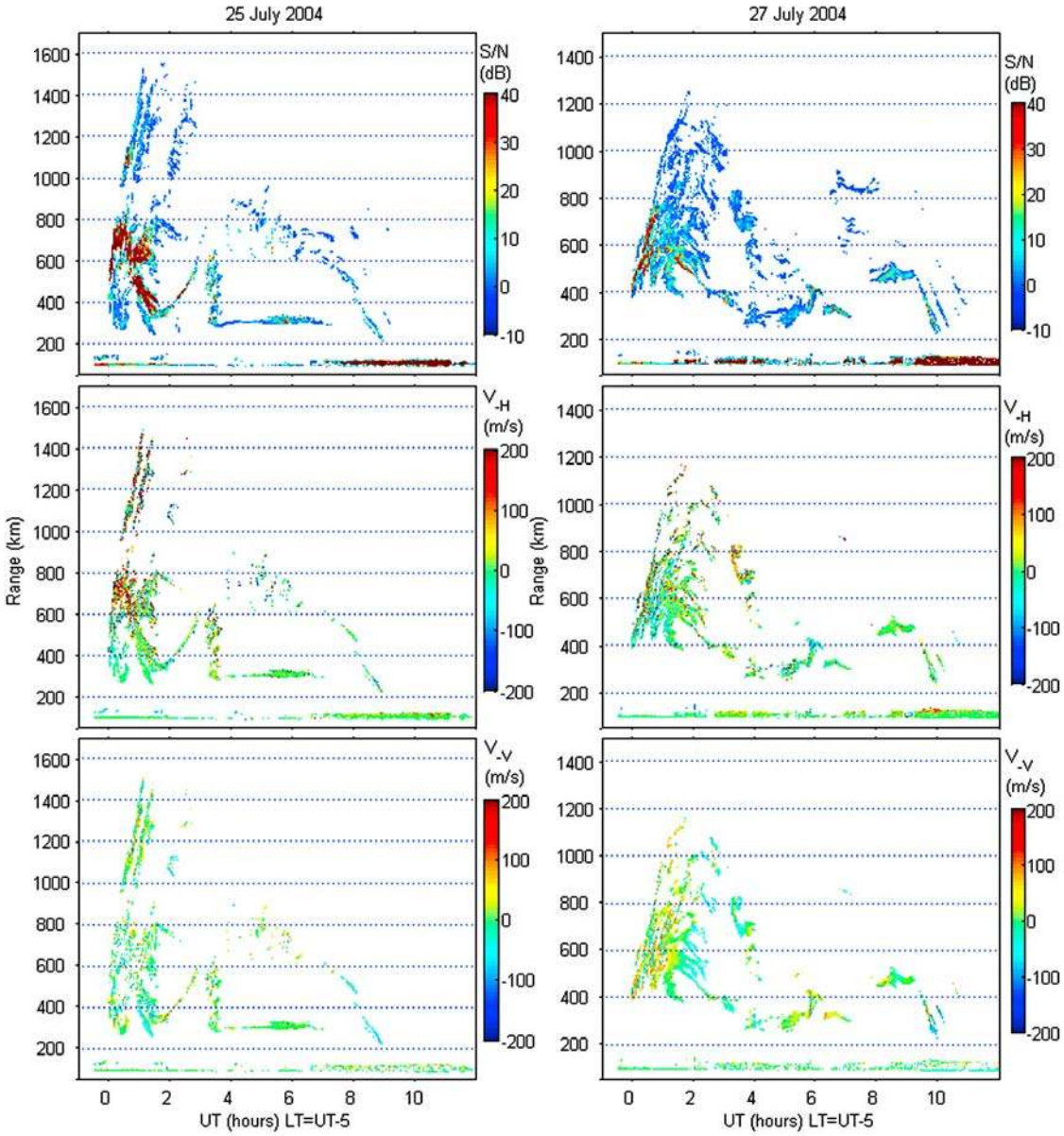

Figure 8. Evolution of equatorial spread *F* observed with the Jicamarca unattended long-term studies of the ionosphere and atmosphere (JULIA) radar. (top) Range-time-intensity plot, showing SNR (dB) versus altitude and universal time (UT). (middle) Zonal and (bottom) vertical drift of the 3 m irregularity velocity.

8, and 10 h, respectively, marked by the horizontal bars in Figure 7. After another increase on 26 July, the spread *F* observed at the three stations began at 2330, 2250, and 2345 UT on 26 July, with durations of 6, 8, and 11 h, respectively.

[14] To determine the altitude extension of the spread *F* irregularities, we employed power maps of coherent echoes collected by the JULIA radar to depict the maximum altitude of the plasma plumes. Figure 8 presents RTI and horizontal and vertical velocity maps from 25 July and 27 July versus UT. Over Jicamarca postsunset plumes and broad spread *F* occur occasionally during the June solstice, as shown in Table 1 of *Chapagain et al.* [2009]. Here the RTI maps show that reflections from *E* layer altitudes persisted throughout the night. Around 0000 UT (1900 LT) on 2 days, reflections detected from bottomside to topside indicate that the irregularities rapidly rose in altitude and exploded into high-altitude plumes. Radar plumes are interpreted as a manifestation of large plasma depletions known as ionospheric PBs that originate in the bottomside *F* region and may extend over a thousand kilometers in altitude [*Sahai et al.*, 2000; *Ma and Maruyama*, 2006; *Huang et al.*, 2007]. The strongest echoes (SNR > 20 dB), which correspond to the presence of the most intense, 3 m spread *F* plasma density irregularities, are observed mainly around 0000–0100 UT (1900–2000 LT) and up to more than 1000 km. The vertical rise velocity for the initial bubbles reaches approximately 100 m s^{-1}. The eastward velocities vary from 100 to 200 m s^{-1}. After that, the

plumes move downward (see the spatial distribution of vertical velocity in the bottom plots in Figure 8) and decay around 0900 UT on 25 July and 1100 UT on 27 July.

[15] At the Brazilian longitude the typical drift velocity is 20 m s^{-1} for the June solstice months, which is insufficient for generation of spread F [*Abdu et al.*, 1981]. It should be noted in Figure 7 that the evening F layer height increase associated with the eastward electric field enhancement on 25 and 27 July is ~25 m s^{-1}. The increased upward vertical drifts and the corresponding F layer uplifts could be arising from the PPEF associated with the southward turning of the IMF and intensification of *AE* that occurred in the dusk sector of the American longitude. This extra push favors the conditions for generation of equatorial irregularities through destabilization of the R-T instability and produces equatorial PBs and plasma bite-outs in the low-occurrence season at the American longitude.

5. Evolution of Irregularities at Southeast Asian/Australian Longitudes

[16] The left plots in Figure 7 show the hmF2 and foF2 variations at Wuhan, Chungli, and Learmonth, located in the Southeast Asian/Australian sector. Significant increases in foF2, which began at around 0400 UT on 25 July, were seen at the low-latitude station Learmonth. However, in the Northern Hemisphere, Wuhan and Chungli witnessed a large decrease in foF2, about 5 MHz (as shown by the shaded area), compared to their quiet-day values, and a significant negative F_2 layer storm prevailed the next day. The hemispheric asymmetry of the electron density enhancement on 25 July was presented by *Pedatella et al.* [2008], using CHAMP in situ density measurements. They attributed this asymmetry to the storm-time equatorward winds as well as changes in the neutral compositions. Strong equatorward winds move the plasma along the magnetic field lines to a higher altitude, where the recombination rate is lower, and then increase the electron density. Taking these observations together, we suggest that the ionospheric disturbance dynamo was active over the Southeast Asian/Australian longitude at midnight of 25 July. When we note the ionograms obtained at Wuhan, Chungli, and Learmonth (not shown here), the spread F started at about 2015, 1900, and 2000 UT, with durations of about 3, 3, and 2 h, respectively. The duration is marked by the horizontal bars in Figure 7. The sample ionograms at Darwin on 25 July are shown in the bottom two left plots Figure 9. They indicate that the observed range-type spread F in the lower part of the F region (RSF-I) seems to be due to the fresh generation of irregularities in the postmidnight hours. After the initiation, the irregularities ascend to higher altitudes and then distribute throughout the whole F region, known as RSF-II [*Chen et al.*, 2006]. These local postmidnight irregularities during magnetically disturbed periods, in general, were considered to be the effects of ionospheric disturbance dynamo electric fields (DDEFs) [*Blanc and Richmond*, 1980; *Fejer and Scherliess*, 1997], which are mainly westward during the local daytime and eastward during the local nighttime. At solar minimum, the nighttime downward drifts are very small [*Fejer et al.*, 1999]. Under such conditions, the vertical drift velocity can easily be reversed by the eastward DDEF, which produces perturbed upward drifts and enhances the R-T instability. Prior to the spread F onset time, the IMF Bz showed a prompt northward turning at ~1550 UT on 25 July, which may also have provided a short-lived in-phase contribution to the disturbance dynamo effects [*Basu et al.*, 2001b] and helped trigger the postmidnight irregularity generation.

[17] The top two plots in Figure 10 illustrate the variations in the amplitude scintillation index S_4 at the L band recorded at Wuhan and West Sumatra (scintillations from all satellites can be found at http://stdb2.stelab.nagoya-u.ac.jp/QL-S4/daily/2004/209_2004_S4.html). The storm on day 27 triggered the development of strong scintillations, which persisted until 2000 UT. As mentioned in section 3, PBs were observed by in situ satellites in Southeast Asian longitudes on this day. These density depletions developed and reached the F region peak, where the plasma density is much higher. Such plasma structures, in an environment of high plasma density, can cause intense amplitude scintillations that adversely impact satellite communication and navigation systems. Figure 10 depicts the scintillation index above the threshold of 0.2. The S_4 index, depending on the electron density deviation of ionospheric irregularities and, also, on the thickness and height of the irregularity layer [*Yeh and Liu*, 1982], quantifies the strength of amplitude scintillation and typically lies in the range of 0 to 1. An impulsive onset of amplitude scintillation occurred at 1230 and 1730 UT, with maximum values of 1 and 0.8 at the Wuhan and West Sumatra stations, respectively. In the L-band frequency range, amplitude scintillations are caused by irregularities at a scale of tens to hundreds of meters, sizes on the order of the first Fresnel zone, $d_F = \sqrt{\lambda(z - L/2)}$, where z is the height of the upper boundary of the irregular layer, and L is the layer thickness [*Wernik et al.*, 2004]. Regarding the GPS TEC the cause of the GPS phase fluctuations (ROTI) is the optical path changes of a radio wave, since the irregularity scale size is much larger than the first Fresnel zone [*Pi et al.*, 1997]. The irregularity scale size for GPS phase fluctuations is a few kilometers for high-elevation angles and tens of kilometers for low-elevation angles [*Aarons*, 1997]. Combining the GPS L-band scintillations and TEC fluctuations, we expect that the small-scale irregularities produced by ionospheric scintillation coexist with the large-scale PB structures at the Southeast Asian/Australian longitude on 27 July. On 25 July no L-band scintillations were observed, although the spread F began postmidnight. By performing a simultaneous irregularity observation by radar and GPS over the Indian region, *Sripathi et al.* [2008] found that neither bottom-type nor postmidnight irregularities give rise to significant L-band scintillations, associated with the detection of dead bubbles, in the postmidnight hours. However, the absence of scintillations on 25 July in our case does not correspond to the preceding situations; instead, perhaps it resulted from the lower ambient electron densities during the postmidnight hours. The gradients at the edges of PBs are small and may not be seen by GPS L-band scintillations.

[18] With regard to ionosonde observations at Wuhan, Chungli, and Learmonth on 27 July, Figure 7 illustrates that prior to the spread F onset time, the hmF2 and foF2 variations at all three stations show a similar wavelike behavior.

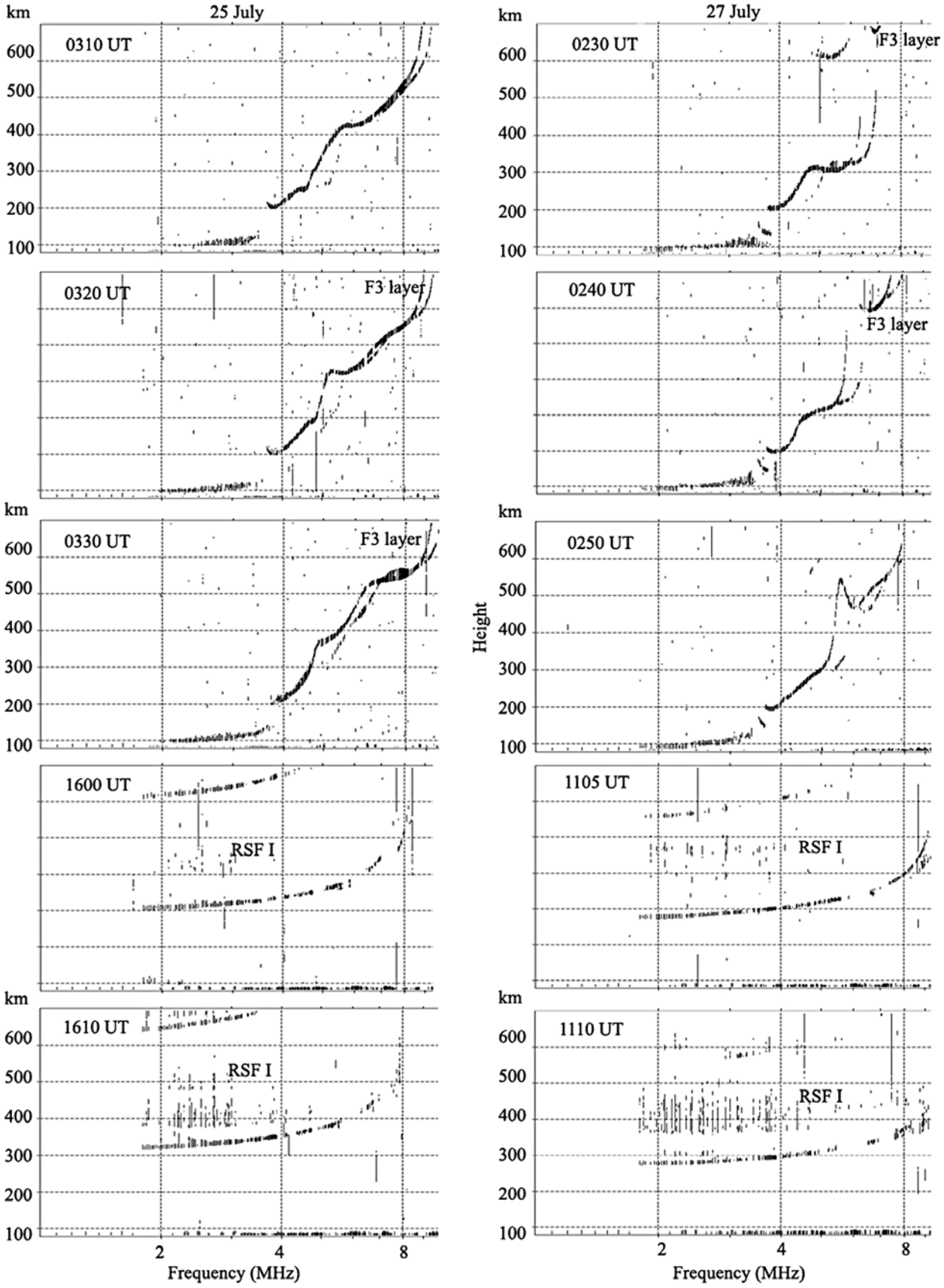

Figure 9. Selected ionograms on (left) 25 July and (right) 27 July showing the occurrence of F_3 layer and type I range spread F (RSF I) at Darwin.

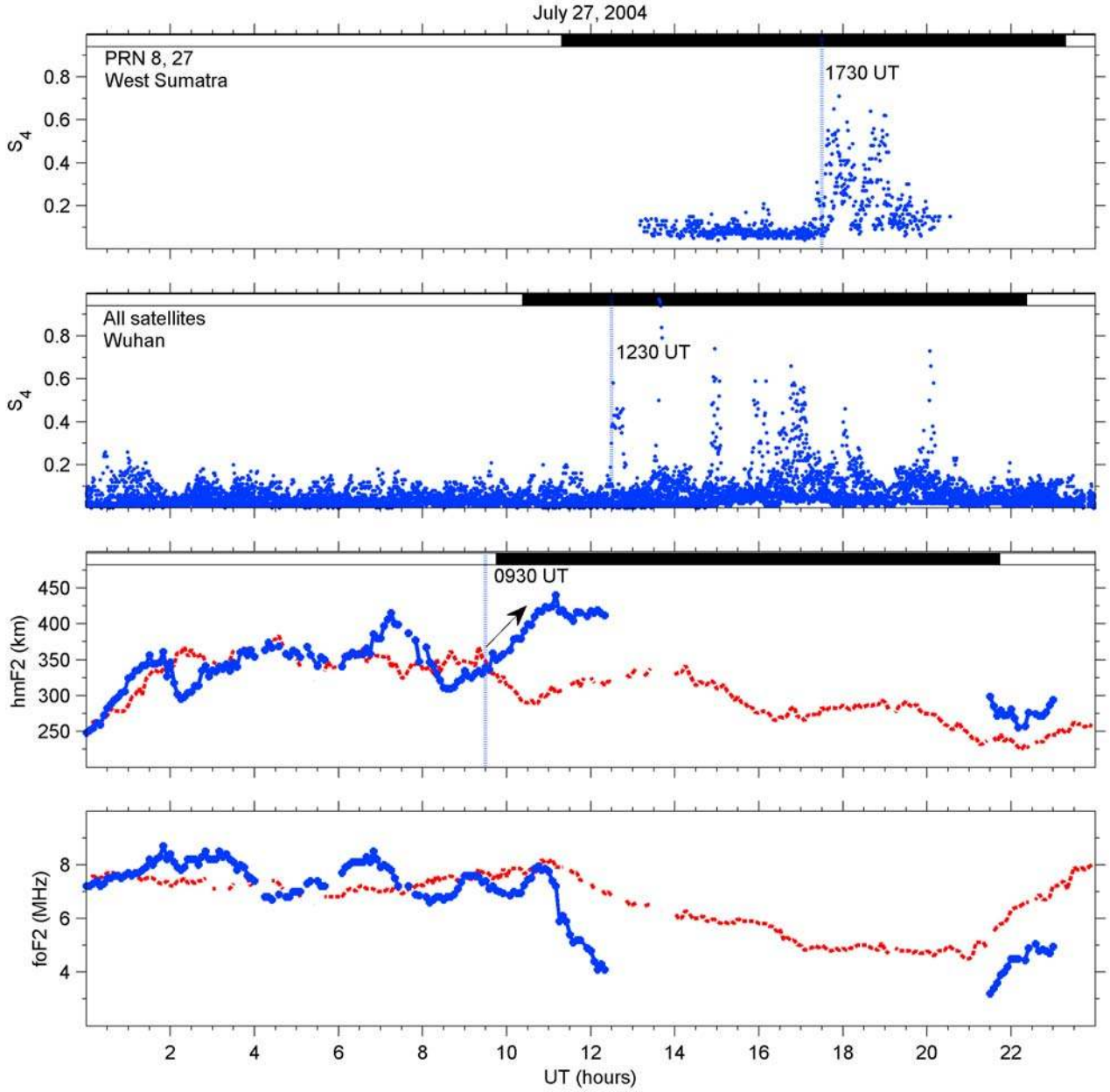

Figure 10. Top two plots show GPS amplitude scintillations observed at West Sumatra and Wuhan. The bottom two plots show variations of the ionospheric hmF2 and foF2 observed at Cebu on 27 July 2004. Red lines are quiet-day (21 July 2004) values. The horizontal bar at the top of each plot indicates daytime (white) and nighttime (black).

A negative correlation of foF2 and hmF2 was observed during the period 0500–1400 UT, probably a TAD effect that originates from the auroral oval region [*Prölss*, 1993]. TADs, which are superimpositions of pulselike or surgelike atmospheric gravity waves, can propagate to equatorial and low latitudes or even into the opposite hemisphere. The passage of these TADs is always associated with a negative correlation or delayed response between hmF2 and foF2, which has been explained through model analysis [e.g., *Bauske and Prölss*, 1997; *Lu et al.*, 2001; *Lee et al.*, 2004; *Lei et al.*, 2008]. Large-scale ESF irregularities related to gravity waves are often observed and modeled [*Kelley and Fukao*, 1991; *Huang et al.*, 1994; *Saito et al.*, 1998]. *Huang and Kelley* [1996] performed nonlinear numerical simulations of gravity waves seeding R-T instability to study the evolution of ESF. They showed that gravity waves initiate the R-T instability in the bottomside *F* region, the instability grows and amplifies the wave-induced perturbations, and finally, PBs occur. Figure 11 depicts the latitudinal TEC fluctuation occurrence sequence at longitudes 146°E (stations CNMR, GUUG, TOW2, and LAE1), 121°E (stations SHAO and TCMS), and 114°E (stations Wuhan and GUAN). Near-simultaneous rapid TEC fluctuations can

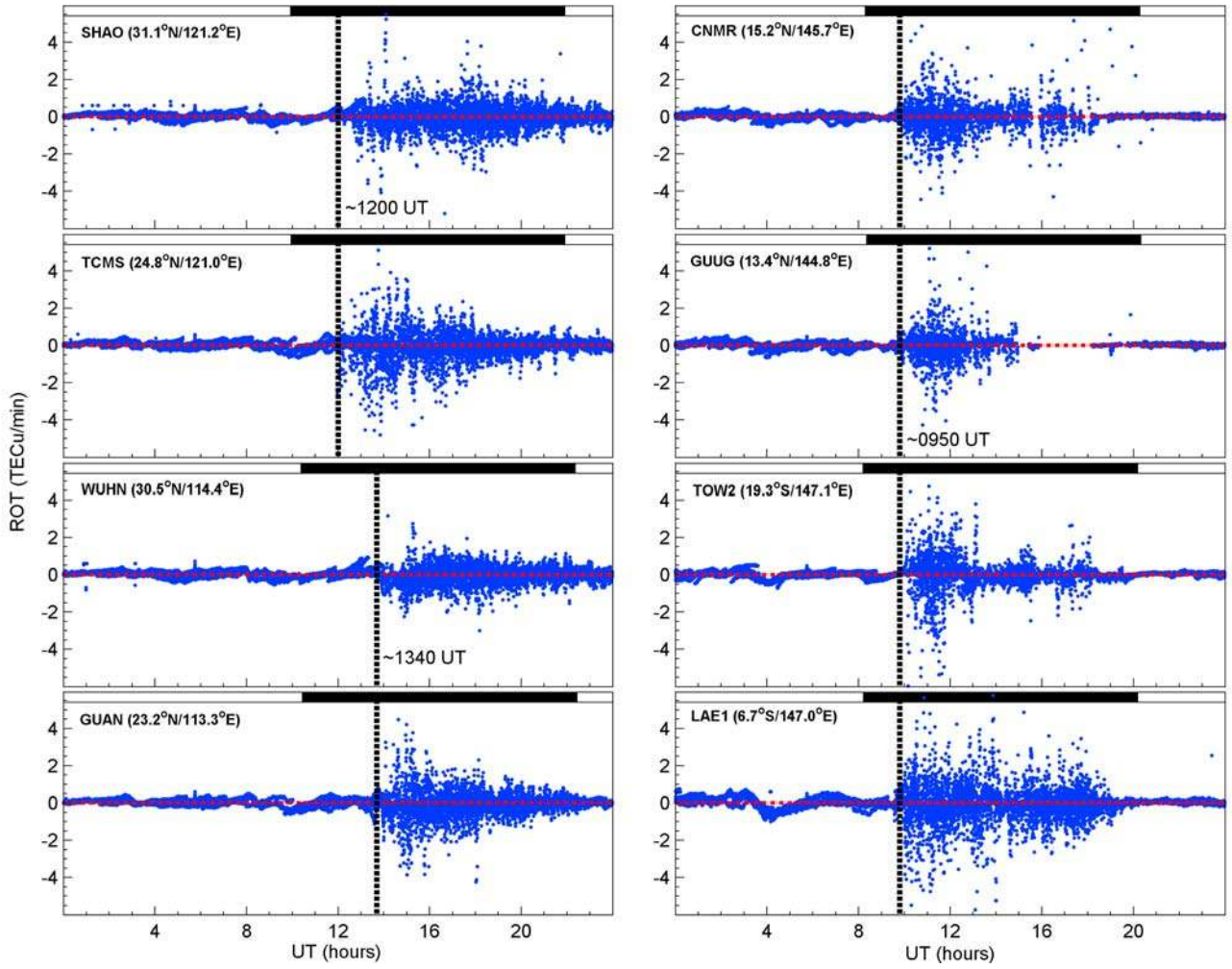

Figure 11. Plots of rate of TEC (ROTI) at the eight selected stations for all satellites on 27 July 2004. The horizontal bar at the top of each plot indicates daytime (white) and nighttime (black).

be seen from the meridional observations at those latitudes around 1000, 1200, and 1400 UT, respectively.

[19] To understand the triggering effects of ionospheric irregularity on 27 July at the Southeast Asian/Australian longitude, hmF2 and foF2 observations from Cebu are shown in the bottom two plots in Figure 10. As is clearly shown, there was an increase in hmF2 at about 75 km, associated with a large upward drift velocity, about 20 m s^{-1} on average, during the period 1000–1100 UT. Several studies have shown that the variation of vertical $\mathbf{E} \times \mathbf{B}$ drift velocity can be estimated from in situ satellite and ionosonde observations [e.g., *Bittencourt and Abdu*, 1981; *Oyekola et al.*, 2008; *Yue et al.*, 2008]. In the equatorial region the *F* layer height is largely determined by the equatorial vertical drift velocity, which is driven by the zonal electric field via the $\mathbf{E} \times \mathbf{B}$ drift [*Dabas et al.*, 2003]. The abrupt increase in hmF2 suggests that an enhanced eastward electric field occurred near postsunset, which resulted from the prompt penetration of the perturbation electric fields at high latitudes to low latitudes [*Sastri et al.*, 1997]. The similar onset times of low-latitude ionospheric irregularities in the Southern and Northern Hemispheres at the Southeast Asian longitude (Figure 11) indicate that the occurrence of PBs could be attributed to the effects of penetration electric fields during the main phase of the storm. It was shown by *Huang et al.* [2007], *Maruyama et al.* [2007], and *Wei et al.* [2008] that penetration electric fields can exist for several to tens of hours as long as the IMF *Bz* remains southward or oscillates between northward and southward directions. As shown in the global PB occurrence map for storm day 27 July (Figure 5), irregularities are sequentially observed from eastern to western longitudes and follow the sunset terminator. In this case eastward penetration electric fields would exist in the evening sector of longitudes from America to Southeast Asia. The enhanced zonal electric field near sunset that occurred nearly in-phase with the prereversal zonal electric field triggered the irregularity development and could have caused an enhancement in the intensity of a developing PB event. At the Southeast Asian longitude, besides the relative strength of the magnetic storm, the local time dependence of PPEFs and DDEFs and the combined triggering effects of postsunset PPEFs and gravity waves appear to be responsible for the situation that the PB occurrence seen at this longitude on 27 July is much wider than that on 25 July. Furthermore, on storm days 25 and 27 July, an F_3 layer

developed at the Australian longitude. Although the F_3 layer is not the theme of this study, the way the storm-time F_3 layer developed and was observed at Darwin is worth mentioning. This is shown by sample ionograms at selected times in Figure 9. As shown in the top plots, a strong F_3 layer developed at the topside ionosphere, beyond the height range of the ionosonde (Figure 9, top right plot). Then this layer drifted downward and had disappeared by ~0300 UT. During geomagnetic storm periods, an F_3 layer was occasionally observed [e.g., *Zhao et al.*, 2005; *Rama Rao et al.*, 2005; *Sreeja et al.*, 2009]; the physical mechanism producing the additional layer has been investigated by *Balan et al.* [1998, 2008] and *Lin et al.* [2009].

6. Conclusions

[20] In this study, multi-instrument data have been analyzed to describe storm-time, low-latitude, *F* region irregularities. We found from ROTI maps and in situ satellites that PBs occurred over a wide longitude extent on storm days 25 and 27 July 2004, from American to Southeast Asian longitudes. Main results of this study include the following.

[21] 1. At the American longitude, ionosonde observations recorded rapid increases in hmF2 at ~2230 UT on 24 July and 2300 UT on 26 July, following the southward turning of the IMF and intensification of *AE*. After that, EIA enhancements and strong range-type spread echoes were observed in the postsunset period, and plasma plumes obtained from radar RTI maps were found to ascend quickly to higher altitudes, >1500 km, associated with PPEFs, thus elevating the *F* layer to a higher altitude and favoring the generation of equatorial irregularities through destabilization of the R-T instability.

[22] 2. The conditions for occurrence of irregularities at the Southeast Asian/Australian longitude on 2 storm days were different. On storm day 25 July the spread *F* was found to begin postmidnight and persist for about 3 h, with an absence of L-band scintillations. The freshly generated postmidnight irregularities are suggested to be associated with DDEFs, which produce perturbed upward drifts and enhance the R-T instability.

[23] 3. On the other storm day we studied, 27 July, the spread *F* occurred postsunset, and near-simultaneous rapid TEC fluctuations could be seen from the meridional observations. Before the spread *F* onset time, ionosonde observations registered TADs passing through this region. On the contrary, hmF2 observations from the equatorial station Cebu showed a rapid increase. These results probably show that the PPEFs, together with gravity wave-seeding effects, induced the irregularities at this longitude on storm day 27 July.

[24] More importantly, the present investigation indicates that during complex storm periods, long-duration or multiple-penetration electric fields [*Tulasi Ram et al.*, 2008] and the combined effects of PPEFs and DDEFs could lead to the development of ESF or PBs over a wide longitudinal extent and/or to their maintenance for a longer duration, which is a serious concern for space-based communication and navigational systems. Further, these results provide some insight into the conditions that may give rise to similar day-to-day variability of ionospheric irregularities over wide longitude regions.

[25] **Acknowledgments.** This research was supported by the Natural Science Foundation of China (40774091, 40574072, 40904038) and National Important Basic Research Project (2006CB806306). The authors acknowledge IGS and UT Dallas for providing the GPS TEC and DMSP F15 density data, respectively. Ionospheric data are from the DIDB and IPS databases. IMF data were obtained from CDAWEB. We thank D. Cooke and C. Roth for processing the CHAMP PLP data. The CHAMP mission is supported by the German Aerospace Center (operation) and the Federal Ministry of Education and Research (data processing). The Jicamarca Radio Observatory is a facility of the Instituto Geofisico del Perú operated with support from NSF Cooperative Agreement ATM-0432565 through Cornell University. J.S.X. was supported by the NSF of China (40874085).

[26] Z. Pu thanks the reviewers for their assistance in evaluating the manuscript.

References

Aarons, J. (1997), Global positioning system phase fluctuations at auroral latitudes, *J. Geophys. Res.*, *102*(A8), 17,219–17,231, doi:10.1029/97JA01118.

Abalde, J. R., Y. Sahai, P. R. Fagundes, F. Becker-Guedes, J. A. Bittencourt, V. G. Pillat, W. L. C. Lima, C. M. N. Candido, and T. F. de Freitas (2009), Day-to-day variability in the development of plasma bubbles associated with geomagnetic disturbances, *J. Geophys. Res.*, *114*, A04304, doi:10.1029/2008JA013788.

Abdu, M. A. (2001), Outstanding problems in the equatorial ionosphere-thermosphere electrodynamics relevant to spread F, *J. Atmos. Sol. Terr. Phys.*, *63*, 869–884, doi:10.1016/S1364-6826(00)00201-7.

Abdu, M. A., I. S. Batista, and J. A. Bittencourt (1981), Some characteristics of spread F at the magnetic equatorial station Fortaleza, *J. Geophys. Res.*, *86*(A8), 6836–6842, doi:10.1029/JA086iA08p06836.

Abdu, M. A., et al. (2008), Abnormal evening vertical plasma drift and effects on ESF and EIA over Brazil-South Atlantic sector during the 30 October 2003 superstorm, *J. Geophys. Res.*, *113*, A07313, doi:10.1029/2007JA012844.

Abdu, M. A., I. S. Batista, B. W. Reinisch, J. R. de Souza, J. H. A. Sobral, T. R. Pedersen, A. F. Medeiros, N. J. Schuch, E. R. de Paula, and K. M. Groves (2009), Conjugate Point Equatorial Experiment (COPEX) campaign in Brazil: Electrodynamics highlights on spread *F* development conditions and day-to-day variability, *J. Geophys. Res.*, *114*, A04308, doi:10.1029/2008JA013749.

Aggson, T. L., W. J. Burke, N. C. Maynard, W. B. Hanson, P. C. Anderson, J. A. Slavin, W. R. Hoegy, and J. L. Saba (1992), Equatorial bubbles updrafting at supersonic speeds, *J. Geophys. Res.*, *97*(A6), 8581–8590, doi:10.1029/92JA00644.

Balan, N., I. S. Batista, M. A. Abdu, J. MacDougall, and G. J. Bailey (1998), Physical mechanism and statistics of occurrence of an additional layer in the equatorial ionosphere, *J. Geophys. Res.*, *103*(A12), 29,169–29,181, doi:10.1029/98JA02823.

Balan, N., S. V. Thampi, K. Lynn, Y. Otsuka, H. Alleyne, S. Watanabe, M. A. Abdu, and B. G. Fejer (2008), F_3 layer during penetration electric field, *J. Geophys. Res.*, *113*, A00A07, doi:10.1029/2008JA013206.

Basu, S., S. Basu, K. M. Groves, H.-C. Yeh, S.-Y. Su, F. J. Rich, P. J. Sultan, and M. J. Keskinen (2001a), Response of the equatorial ionosphere in the South Atlantic region to the Great Magnetic Storm of July 15, 2000, *Geophys. Res. Lett.*, *28*(18), 3577–3580, doi:10.1029/2001GL013259.

Basu, S., et al. (2001b), Ionospheric effects of major magnetic storms during the International Space Weather Period of September and October 1999: GPS observations, VHF/UHF scintillations, and in situ density structures at middle and equatorial latitudes, *J. Geophys. Res.*, *106*(A12), 30,389–30,413, doi:10.1029/2001JA001116.

Basu, S., S. Basu, K. M. Groves, E. MacKenzie, M. J. Keskinen, and F. J. Rich (2005), Near-simultaneous plasma structuring in the midlatitude and equatorial ionosphere during magnetic superstorms, *Geophys. Res. Lett.*, *32*, L12S05, doi:10.1029/2004GL021678.

Basu, S., S. Basu, J. Huba, J. Krall, S. E. McDonald, J. J. Makela, E. S. Miller, S. Ray, and K. Groves (2009), Day-to-day variability of the equatorial ionization anomaly and scintillations at dusk observed by GUVI and modeling by SAMI3, *J. Geophys. Res.*, *114*, A04302, doi:10.1029/2008JA013899.

Bauske, R., and G. W. Prölss (1997), Modeling the ionospheric response to traveling atmospheric disturbances, *J. Geophys. Res.*, *102*, 14,555–14,562, doi:10.1029/97JA00941.

Bhattacharyya, A., T. L. Beach, S. Basu, and P. M. Kintner (2000), Nighttime equatorial ionosphere: GPS scintillations and differential carrier phase fluctuations, *Radio Sci.*, *35*(1), 209–224, doi:10.1029/1999RS002213.

Bittencourt, J. A., and M. A. Abdu (1981), A theoretical comparison between apparent and real vertical ionization drift velocities in the equatorial F region, *J. Geophys. Res.*, *86*(A4), 2451–2454, doi:10.1029/JA086iA04p02451.

Blanc, M., and A. D. Richmond (1980), The ionospheric disturbance dynamo, *J. Geophys. Res.*, *85*(A4), 1669–1686, doi:10.1029/JA085iA04p01669.

Briggs, B. H., and I. A. Parkin (1963), On the variation of radio star and satellite scintillation with zenith angle, *J. Atmos. Terr. Phys.*, *25*, 339–365, doi:10.1016/0021-9169(63)90150-8.

Burke, W. J., L. C. Gentile, C. Y. Huang, C. E. Valladares, and S. Y. Su (2004), Longitudinal variability of equatorial plasma bubbles observed by DMSP and ROCSAT-1, *J. Geophys. Res.*, *109*, A12301, doi:10.1029/2004JA010583.

Chapagain, N. P., B. G. Fejer, and J. L. Chau (2009), Climatology of postsunset equatorial spread *F* over Jicamarca, *J. Geophys. Res.*, *114*, A07307, doi:10.1029/2008JA013911.

Chen, W. S., C. C. Lee, J. Y. Liu, F. D. Chu, and B. W. Reinisch (2006), Digisonde spread *F* and GPS phase fluctuations in the equatorial ionosphere during solar maximum, *J. Geophys. Res.*, *111*, A12305, doi:10.1029/2006JA011688.

Dabas, R. S., L. Singh, D. R. Lakshmi, P. Subramanyam, P. Chopra, and S. C. Garg (2003), Evolution and dynamics of equatorial plasma bubbles: Relationships to ExB drift, postsunset total electron content enhancements, and equatorial electrojet strength, *Radio Sci.*, *38*(4), 1075, doi:10.1029/2001RS002586.

Dandekar, B. S., and K. M. Groves (2004), Using ionospheric scintillation observations for studying the morphology of equatorial ionospheric bubbles, *Radio Sci.*, *39*, RS3010, doi:10.1029/2003RS003020.

Ding, F., W. Wan, L. Liu, E. L. Afraimovich, S. V. Voeykov, and N. P. Perevalova (2008), A statistical study of large-scale traveling ionospheric disturbances observed by GPS TEC during major magnetic storms over the years 2003–2005, *J. Geophys. Res.*, *113*, A00A01, doi:10.1029/2008JA013037.

Fejer, B. G., and L. Scherliess (1997), Empirical models of storm time equatorial zonal electric fields, *J. Geophys. Res.*, *102*(A11), 24,047–24,056, doi:10.1029/97JA02164.

Fejer, B. G., L. Scherliess, and E. R. de Paula (1999), Effects of the vertical plasma drift velocity on the generation and evolution of equatorial spread *F*, *J. Geophys. Res.*, *104*(A9), 19,859–19,869, doi:10.1029/1999JA900271.

Fukao, S., Y. Ozawa, M. Yamamoto, and R. T. Tsunoda (2003), Altitude-extended equatorial spread *F* observed near sunrise terminator over Indonesia, *Geophys. Res. Lett.*, *30*(22), 2137, doi:10.1029/2003GL018383.

Huang, C.-S. (2008), Continuous penetration of the interplanetary electric field to the equatorial ionosphere over eight hours during intense geomagnetic storms, *J. Geophys. Res.*, *113*, A11305, doi:10.1029/2008JA013588.

Huang, C.-S., and M. C. Kelley (1996), Nonlinear evolution of equatorial spread *F*: 3. Plasma bubbles generated by structured electric fields, *J. Geophys. Res.*, *101*(A1), 303–313, doi:10.1029/95JA02209.

Huang, C.-S., C. A. Miller, and M. C. Kelley (1994), Basic properties and gravity wave initiation of the midlatitude *F* region instability, *Radio Sci.*, *29*(1), 395–405, doi:10.1029/93RS01669.

Huang, C.-S., J. C. Foster, and M. C. Kelley (2005), Long-duration penetration of the interplanetary electric field to the low-latitude ionosphere during the main phase of magnetic storms, *J. Geophys. Res.*, *110*, A11309, doi:10.1029/2005JA011202.

Huang, C.-S., J. C. Foster, and Y. Sahai (2007), Significant depletions of the ionospheric plasma density at middle latitudes: A possible signature of equatorial spread *F* bubbles near the plasmapause, *J. Geophys. Res.*, *112*, A05315, doi:10.1029/2007JA012307.

Huang, C. Y., W. J. Burke, J. S. Machuzak, L. C. Gentile, and P. J. Sultan (2001), DMSP observations of equatorial plasma bubbles in the topside ionosphere near solar maximum, *J. Geophys. Res.*, *106*(A5), 8131–8142, doi:10.1029/2000JA000319.

Huba, J. D., and G. Joyce (2007), Equatorial spread *F* modeling: Multiple bifurcated structures, secondary instabilities, large density "bite-outs," and supersonic flows, *Geophys. Res. Lett.*, *34*, L07105, doi:10.1029/2006GL028519.

Hysell, D. L., and J. D. Burcham (1998), JULIA radar studies of equatorial spread F, *J. Geophys. Res.*, *103*(A12), 29,155–29,167, doi:10.1029/98JA02655.

Kelley, M. C. (1989), The Earth's Ionosphere: Plasma Physics and Electrodynamics, *Int. Geophys. Ser.*, vol. 43, Academic, San Diego, Calif.

Kelley, M. C., and S. Fukao (1991), Turbulent upwelling of the mid-latitude ionosphere: 2. Theoretical framework, *J. Geophys. Res.*, *96*(A3), 3747–3753, doi:10.1029/90JA02252.

Kikuchi, T., H. Liihr, K. Schlegel, H. Tachihara, M. Shinohara, and T.-I. Kitamura (2000), Penetration of auroral electric fields to the equator during a substorm, *J. Geophys. Res.*, *105*(A10), 23,251–23,261, doi:10.1029/2000JA900016.

Kil, H., and R. A. Heelis (1998a), Equatorial density irregularity structures at intermediate scales and their temporal evolution, *J. Geophys. Res.*, *103*(A3), 3969–3981, doi:10.1029/97JA03344.

Kil, H., and R. A. Heelis (1998b), Global distribution of density irregularities in the equatorial ionosphere, *J. Geophys. Res.*, *103*(A1), 407–417, doi:10.1029/97JA02698.

Kil, H., L. J. Paxton, S.-Y. Su, Y. Zhang, and H. Yeh (2006), Characteristics of the storm-induced big bubbles (SIBBs), *J. Geophys. Res.*, *111*, A10308, doi:10.1029/2006JA011743.

Lee, C.-C., J.-Y. Liu, M.-Q. Chen, S.-Y. Su, H.-C. Yeh, and K. Nozaki (2004), Observation and model comparisons of the traveling atmospheric disturbances over the Western Pacific region during the 6–7 April 2000 magnetic storm, *J. Geophys. Res.*, *109*, A09309, doi:10.1029/2003JA010267.

Lee, C. C., F. D. Chu, W. S. Chen, J. Y. Liu, S.-Y. Su, Y. A. Liou, and S. B. Yu (2009), Spread F, GPS phase fluctuations, and plasma bubbles near the crest of equatorial ionization anomaly during solar maximum, *J. Geophys. Res.*, *114*, A08302, doi:10.1029/2009JA014195.

Lei, J., A. G. Burns, T. Tsugawa, W. Wang, S. C. Solomon, and M. Wiltberger (2008), Observations and simulations of quasiperiodic ionospheric oscillations and large-scale traveling ionospheric disturbances during the December 2006 geomagnetic storm, *J. Geophys. Res.*, *113*, A06310, doi:10.1029/2008JA013090.

Li, G., B. Ning, L. Liu, Z. Ren, J. Lei, and S.-Y. Su (2007), The correlation of longitudinal/seasonal variations of evening equatorial pre-reversal drift and of plasma bubbles, *Ann. Geophys.*, *25*, 2571–2578.

Li, G., B. Ning, B. Zhao, L. Liu, W. Wan, F. Ding, J. S. Xu, J. Y. Liu, and K. Yumoto (2009), Characterizing the 10 November 2004 storm-time middle-latitude plasma bubble event in Southeast Asia using multi-instrument observations, *J. Geophys. Res.*, *114*, A07304, doi:10.1029/2009JA014057.

Lin, C. H., A. D. Richmond, J. Y. Liu, G. J. Bailey, and B. W. Reinisch (2009), Theoretical study of new plasma structures in the low-latitude ionosphere during a major magnetic storm, *J. Geophys. Res.*, *114*, A05303, doi:10.1029/2008JA013951.

Lu, G., A. D. Richmond, R. G. Roble, and B. A. Emery (2001), Coexistence of ionospheric positive and negative storm phase under northern winter conditions: A case study, *J. Geophys. Res.*, *106*, 24,493–24,504, doi:10.1029/2001JA000003.

Ma, G., and T. Maruyama (2006), A super bubble detected by dense GPS network at east Asian longitudes, *Geophys. Res. Lett.*, *33*, L21103, doi:10.1029/2006GL027512.

Martinis, C. R., M. J. Mendillo, and J. Aarons (2005), Toward a synthesis of equatorial spread *F* onset and suppression during geomagnetic storms, *J. Geophys. Res.*, *110*, A07306, doi:10.1029/2003JA010362.

Maruyama, N., S. Sazykin, R. W. Spiro, D. Anderson, A. Anghel, R. A. Wolf, F. R. Toffoletto, T. J. Fuller-Rowell, M. V. Codrescu, and A. D. Richmond (2007), Modeling storm-time electrodynamics of the low latitude ionosphere-thermosphere system: Can long lasting disturbance electric fields be accounted for? *J. Atmos. Sol. Terr. Phys.*, *69*, 1182–1199, doi:10.1016/j.jastp.2006.08.020.

McClure, J. P., S. Singh, D. K. Bamgboye, F. S. Johnson, and H. Kil (1998), Occurrence of equatorial F region irregularities: Evidence for tropospheric seeding, *J. Geophys. Res.*, *103*(A12), 29,119–29,135, doi:10.1029/98JA02749.

McNamara, L. F., D. L. Cooke, C. E. Valladares, and B. W. Reinisch (2007), Comparison of CHAMP and Digisonde plasma frequencies at Jicamarca, Peru, *Radio Sci.*, *42*, RS2005, doi:10.1029/2006RS003491.

Nishioka, M., A. Saito, and T. Tsugawa (2008), Occurrence characteristics of plasma bubble derived from global ground-based GPS receiver networks, *J. Geophys. Res.*, *113*, A05301, doi:10.1029/2007JA012605.

Oyekola, O. S., A. Ojo, and J. Akinrimisi (2008), A comparison of ground and satellite observations of *F* region vertical velocity near the dip equator, *Radio Sci.*, *43*, RS1005, doi:10.1029/2007RS003699.

Park, J., K. W. Min, V. P. Kim, H. Kil, J.-J. Lee, H.-J. Kim, E. Lee, and D. Y. Lee (2005), Global distribution of equatorial plasma bubbles in the premidnight sector during solar maximum as observed by KOMPSAT-1 and Defense Meteorological Satellite Program F15, *J. Geophys. Res.*, *110*, A07308, doi:10.1029/2004JA010817.

Pedatella, N. M., J. M. Forbes, J. Lei, J. P. Thayer, and K. M. Larson (2008), Changes in the longitudinal structure of the low-latitude iono-

sphere during the July 2004 sequence of geomagnetic storms, *J. Geophys. Res.*, *113*, A11315, doi:10.1029/2008JA013539.

Pi, X., A. J. Mannucci, U. J. Lindqwister, and C. M. Ho (1997), Monitoring of global ionospheric irregularities using the Worldwide GPS Network, *Geophys. Res. Lett.*, *24*(18), 2283–2286, doi:10.1029/97GL02273.

Prölss, G. W. (1993), Common origin of positive ionospheric storms at middle latitudes and the geomagnetic activity effect at low latitudes, *J. Geophys. Res.*, *98*, 5981–5991, doi:10.1029/92JA02777.

Rama Rao, P. V. S., K. Niranjan, D. S. V. V. D. Prasad, P. S. Brahmanandam, and S. Gopikrishna (2005), Features of additional stratification in ionospheric F_2 layer observed for half a solar cycle over Indian low latitudes, *J. Geophys. Res.*, *110*, A04307, doi:10.1029/2004JA010646.

Rich, F. J., and M. Hairston (1994), Large-scale convection patterns observed by DMSP, *J. Geophys. Res.*, *99*(A3), 3827–3844, doi:10.1029/93JA03296.

Rodrigues, F. S., E. R. de Paula, M. A. Abdu, A. C. Jardim, K. N. Iyer, P. M. Kintner, and D. L. Hysell (2004), Equatorial spread *F* irregularity characteristics over São Luís, Brazil, using VHF radar and GPS scintillation techniques, *Radio Sci.*, *39*, RS1S31, doi:10.1029/2002RS002826.

Sahai, Y., P. R. Fagundes, and J. A. Bittencourt (2000), Transequatorial F region ionospheric plasma bubbles: Solar cycle effects, *J. Atmos. Sol. Terr. Phys.*, *62*, 1377–1383, doi:10.1016/S1364-6826(00)00179-6.

Sahai, Y., P. R. Fagundes, J. R. Abalde, A. A. Pimenta, J. A. Bittencourt, Y. Otsuka, and V. H. Rios (2004), Generation of large-scale equatorial *F* region plasma depletions during low range spread-F season, *Ann. Geophys.*, *22*, 15–23.

Sahai, Y., et al. (2005), Effects of the major geomagnetic storms of October 2003 on the equatorial and low-latitude *F* region in two longitudinal sectors, *J. Geophys. Res.*, *110*, A12S91, doi:10.1029/2004JA010999.

Saito, A., T. Iyemori, and M. Takeda (1998), Evolutionary process of 10 kilometer scale irregularities in the nighttime midlatitude ionosphere, *J. Geophys. Res.*, *103*(A3), 3993–4000, doi:10.1029/97JA02517.

Sastri, J. H., M. A. Abdu, I. S. Batista, and J. H. A. Sobral (1997), Onset conditions of equatorial (range) spread *F* at Fortaleza, Brazil, during the June solstice, *J. Geophys. Res.*, *102*(A11), 24,013–24,021, doi:10.1029/97JA02166.

Sreeja, V., C. V. Devasia, S. Ravindran, T. K. Pant, and R. Sridharan (2009), Response of the equatorial and low-latitude ionosphere in the Indian sector to the geomagnetic storms of January 2005, *J. Geophys. Res.*, *114*, A06314, doi:10.1029/2009JA014179.

Sripathi, S., S. Bose, A. K. Patra, T. K. Pant, B. Kakad, and A. Bhattacharyya (2008), Simultaneous observations of ESF irregularities over Indian region using radar and GPS, *Ann. Geophys.*, *26*, 3197–3213.

Su, S.-Y., C. H. Liu, H. H. Ho, and C. K. Chao (2006), Distribution characteristics of topside ionospheric density irregularities: Equatorial versus midlatitude regions, *J. Geophys. Res.*, *111*, A06305, doi:10.1029/2005JA011330.

Su, S.-Y., C. K. Chao, and C. H. Liu (2008), On monthly/seasonal/longitudinal variations of equatorial irregularity occurrences and their relationship with the postsunset vertical drift velocities, *J. Geophys. Res.*, *113*, A05307, doi:10.1029/2007JA012809.

Sultan, P. J. (1996), Linear theory and modeling of the Rayleigh-Taylor instability leading to the occurrence of equatorial spread *F*, *J. Geophys. Res.*, *101*(A12), 26,875–26,891, doi:10.1029/96JA00682.

Tsunoda, R. T. (2006), Day-to-day variability in equatorial spread *F*: Is there some physics missing? *Geophys. Res. Lett.*, *33*, L16106, doi:10.1029/2006GL025956.

Tulasi Ram, S., P. V. S. Rama Rao, D. S. V. V. D. Prasad, K. Niranjan, S. Gopi Krishna, R. Sridharan, and S. Ravindran (2008), Local time dependent response of postsunset ESF during geomagnetic storms, *J. Geophys. Res.*, *113*, A07310, doi:10.1029/2007JA012922.

Van Zandt, T. E., V. L. Peterson, and A. R. Laird (1971), Electromagnetic drift of the midlatitude F_2 layer during a storm, *J. Geophys. Res.*, *76*(1), 278–281, doi:10.1029/JA076i001p00278.

Wei, Y., M. Hong, W. Wan, A. Du, J. Lei, B. Zhao, W. Wang, Z. Ren, and X. Yue (2008), Unusually long-lasting multiple penetration of interplanetary electric field to equatorial ionosphere under oscillating IMF, *Geophys. Res. Lett.*, *35*, L02102, doi:10.1029/2007GL032305.

Wernik, A. W., L. Alfonsi, and M. Materassi (2004), Ionospheric irregularities, scintillation and its effect on system, Acta Geophys. *Polonica*, *52*(2), 237–249.

Yeh, K. C., and C. H. Liu (1982), Radio wave scintillation in the ionosphere, *IEEE Proc.*, *70*, 324–360, doi:10.1109/PROC.1982.12313.

Yue, X., W. Wan, J. Lei, and L. Liu (2008), Modeling the relationship between $\mathbf{E} \times \mathbf{B}$ vertical drift and the time rate of change of hmF2 (DhmF2/Dt) over the magnetic equator, Beijing *Geophys. Res. Lett.*, *35*, L05104, doi:10.1029/2007GL033051.

Zhang, J., et al. (2007), Solar and interplanetary sources of major geomagnetic storms ($Dst \leq -100$ nT) during 1996–2005, *J. Geophys. Res.*, *112*, A10102, doi:10.1029/2007JA012321.

Zhao, B., W. Wan, and L. Liu (2005), Responses of equatorial anomaly to the October–November 2003 superstorms, *Ann. Geophys.*, *23*, 693–706.

L. Hu, G. Li, L. Liu, B. Ning, W. Wan, X. Yue, and B. Zhao, Beijing National Observatory of Space Environment, Institute of Geology and Geophysics, Chinese Academy of Sciences, Beijing 100101, China. (GZLee@mail.iggcas.ac.cn)

K. Igarashi and M. Kubota, National Institute of Information and Communications Technology, 4-2-1 Nukui-Kitamachi, Koganei, Tokyo 184-8795, Japan.

J. Y. Liu, Institute of Space Science, National Central University, 300 Jungda Rd., Chung-Li, Taiwan 32001.

Y. Otsuka, Solar-Terrestrial Environment Laboratory, Nagoya University, Furo-cho, Chikusa-ku, Nagoya, Aichi 464-8601, Japan.

J. S. Xu, School of Electronic Information, Wuhan University, Wuhan 430079, China.